12th Brazilian Congress of Manufacturing Engineering
May 10th-12th, 2023, Brasilia, DF, Brazil

MATERIAL IDENTIFICATION IN HELICAL MILLING FOR SMART DRILLING APPLICATIONS

Sughosh Deshpande
Abdallah Bouzid
Pierre Lagarrigue
Yann Landon
Anna Carla Araujo
Institut Clément Ader, Université de Toulouse, CNRS/INSA/ISAE/Mines Albi/UPS, France
sughosh.deshpande@univ-tlse3.fr
abdallah.bouzid@univ-tlse3.fr
pierre.lagarrigue@univ-jfc.fr
yann.landon@univ-tlse3.fr
araujo@insa-toulouse.fr

Abstract. *Hole making on stacked aerospace materials is a major operation during aircraft assembly which poses significant challenges during manufacturing because of different material machinability. Most common problems include poor hole quality and low productivity as single tool and same cutting parameter is used for both material layers. Strategies involving smart machining including adapting proper cutting conditions by real time data monitoring can have significant improvements. Data map of specific coefficients is developed for material identification during orbital drilling of stacked Aluminium and Titanium alloys by monitoring machine spindle power, spindle and cutting flute position . Our result shows the applicability of data map technique consisting of axial cutting coefficients K_{ab} for material identification in orbital drilling by monitoring machine spindle power and spindle position.*

Keywords: *Smart machining. Aerospace stacks. Data monitoring. Spindle power. CNC internal sensors.*

1. INTRODUCTION

Industry 4.0 is the need of the hour in current global market scenario and all the processes are moving towards automation and smart manufacturing. The data exchange between different systems in the factory is of primary importance in order to correct and adapt to real time circumstances by decision making. The use of OPC UA (Open Platform Communication Unified Architecture) and MT connect based platforms to exchange data between machine tools and clients is demonstrated by Liu *et al.* (2019). The IoT based predictive maintenance of CNC machines by real time condition monitoring is demonstrated by Al-Naggar *et al.* (2021).

The hardware and techniques required for data monitoring and acquisition should be feasible enough for easy implementation on the shop floor without expensive investments and disturbance to current processes (Axinte and Gindy, 2004). The machine data from the modern day CNC machines can have significant value and are also easy to acquire without any additional accessories or hardware setup (Lauro *et al.*, 2014). The internal sensors in the machine tool capture variety of data which can be useful for the operator to improve productivity and tool life for a particular machining process. Cutting tool condition monitoring using machine internal sensors is demonstrated by Demko *et al.* (2022).

Modern day airplanes are made of multiple light weight high performance materials to achieve better fuel efficiency and reliability (Boyer *et al.*, 2015). This also includes using stacked layers of Aluminium, Titanium and CFRP especially in the wings and air frames where thousands of holes have to be drilled before final assembly. Aerospace stack hole making is an application where lot of research is being carried out in order to enhance the process productivity and hole quality (Zhaoju *et al.*, 2017; Vijayan *et al.*, 2010). Each of the material layer in a stack has different machinability and using one common tool for hole-making in both the layers is a challenge which results in poor hole quality and lower productivity. Also, changing the tool geometry suitable for each layer during the drilling process is not practically advisable. The idea of adapting right cutting conditions for each material layer in real time by a single tool can be feasible by implementation of smart machining strategies involving data acquisition, monitoring and feedback (Araujo *et al.*, 2021).

Orbital drilling is a helical milling process where in the tool moves simultaneously in X,Y and Z positions resulting in material removal at bottom and peripheral cutting edges of the end mill. Numerous articles have compared different quality aspects of holes produced during helical milling and axial drilling (Ge *et al.*, 2022; Dan Sun, 2018; **?**). Some of the quality aspects include burr height, surface finish and fatigue life of the produced holes which are crucial for

aerospace applications. Better chip evacuation, lesser forces result in better tool life and hole quality in helical milling. Implementation of helical milling for producing holes in aerospace stacks is also widely researched topic and considerable work is being done in this area (Wang *et al.*, 2018; Denkena *et al.*, 2008).

Precise real time material identification along with instantaneous correction in cutting condition if required is crucial for successful implementation of smart machining strategies. Fang *et al.* (2015) developed force sensor less method to detect stack interface in robotic orbital drilling operations which can be helpful to adapt proper cutting conditions. The identification of process incidences during stack drilling by assessing different decision making algorithms is demonstrated by Pardo *et al.* (2021). Monitoring of signals from AE sensors for tool position identification in CFRP/Aluminium stacks is shown by Neugebauer *et al.* (2012). Our recent work demonstrated material identification during circular milling by development of data maps of specific cutting coefficients in Aluminium and Titanium alloys by online monitoring of cutting forces (Deshpande *et al.*, 2022a).

The goal of this paper is to analyse and verify the applicability of data maps in helical milling of stacked Aluminium and Titanium alloys for real time material identification. This is achieved by monitoring machine spindle power and calculating specific cutting coefficients to distinguish the materials in the stack. Our work also proposes and verifies the possibility of utilizing CNC machine internal sensors for online data monitoring which can be advantageous compared to using external expensive sensors like force dynamometers.

In the following sections, the machining force model is presented and identification of the cutting coefficients methodology in helical milling is reviewed, followed by experimental set-up used in this research. The cutting forces and power results are presented and discussed, and lastly, the identification map with cutting coefficients derived by monitoring spindle power are presented.

2. HELICAL MILLING

2.1 Process kinematics

In orbital drilling, the milling tool follows a helical trajectory as shown in Fig. 1(a). The combination of tool movement in XY plane and Z plane simultaneously results in gradual removal of material for every orbital rotation of the tool (Eq. 1). The depth of material removed per orbital rotation is designated as pitch P (mm/rev) and it is a function of the feed and the radius of the trajectory R_{tt}, calculated based on the tool diameter D_t and the machined diameter D (Eq. 2). The resulting ramp angle is indicated as α (Eq. 3), a function of the axial feed and the circular feed (Wang *et al.*, 2012).

$$\vec{f_z} = \vec{f_{xy}}(xy\ plane) + \vec{f_a}(axial) \tag{1}$$

$$P = \frac{f_a\ 2\pi R_{tt}}{f_{xy}} = \frac{f_a\ \pi(D - D_t)}{f_{xy}} \tag{2}$$

$$\alpha = \arctan\frac{P}{\pi(D-D_t)} = \arctan\frac{f_a}{f_{xy}} \tag{3}$$

$$N_{orb} = \frac{f_a\ Z\ N}{P} \tag{4}$$

Figure 1(b) shows tool trajectory with reference to work piece (X_m, Y_m) and tool (X_t,Y_t) referential frames. The tool rotates around its own axis at N(rpm) spindle speed (or $\dot{\theta}_2$ rad/s) and around hole center O at N_{orb} rpm (or $\dot{\theta}_1$ rad/s) to machine the hole. The offset distance between tool center C and hole center O is designated as R_{tt}.

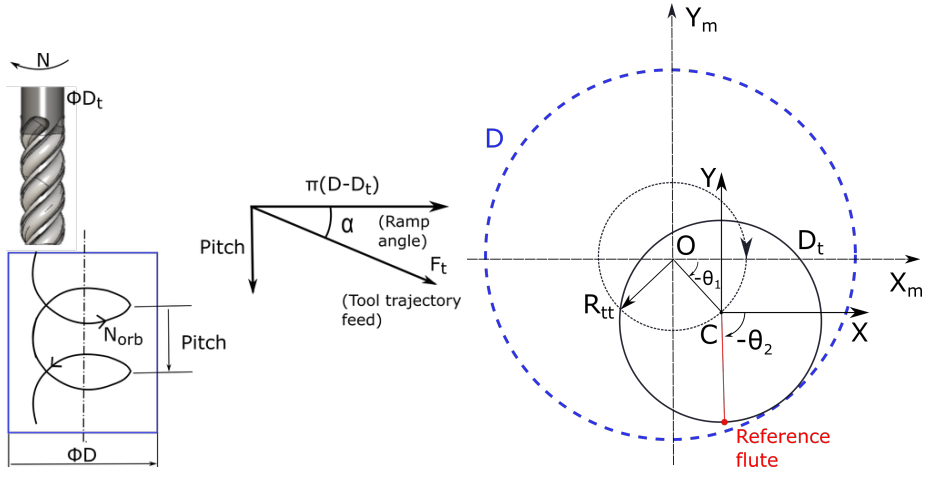

(a) Helical milling parameters (b) Referential frames in X and Y

Figure 1: Tool trajectory in orbital drilling

2.2 Analysis of uncut chip geometry for force modelling

The uncut chip geometry and prediction of cutting forces in helical milling is discussed by recent articles (Rey *et al.*, 2016; Wang *et al.*, 2018). In case of end milling, there are two zones of chip generation: at the peripheral edge, that it is represented by the index 'p' in this article, and the bottom edge of the tool, represented by 'b' index.

In the periphery, the chip width b_p is a function of θ_2 and the axial position of the tool in the orbital rotation (Shang *et al.*, 2018) and the chip thickness h_p is described by Martellotti equation (Martellotti, 1941):

$$b_p(\theta_2) = P - \frac{P}{\pi} \arccos \frac{R_{tt} - R_t \cos(\theta_2)}{\sqrt{R_{tt}^2 + R_t^2 - 2R_t R_{tt} \cos(\theta_2)}} \tag{5}$$

$$h_p(\theta_2) = f_z \sin(\theta_2) \tag{6}$$

$$b_b = \frac{D_t}{2} \tag{7}$$

$$h_b = f_z \frac{P}{\pi(D - D_t)} \tag{8}$$

In the bottom edge, the chip length b_b can be approximated to tool radius (Eq. 7) and the chip thickness is described by Eq. 8. The bottom uncut chip thickness can be assumed constant and independent of cutting velocity. The secondary cutting edge can be assumed to have zero position angle. The specific force coefficients can be identified for the bottom edge and peripheral edge of the tool based on the local uncut chip load. Figure 2(a) shows chip generation during orbital milling.

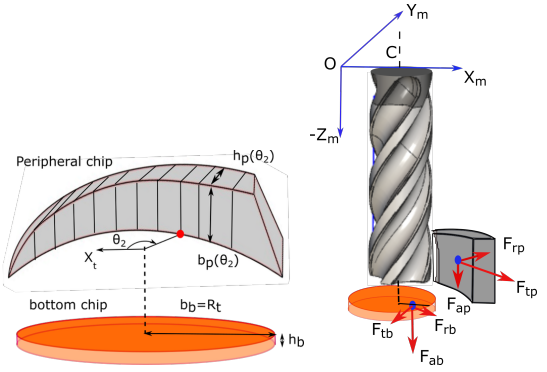

(a) Uncut chip geometry (b) Cutting forces at periphery and bottom edges

Figure 2: Chip generation and cutting forces during helical milling

2.3 Cutting forces and specific force coefficients

The mechanistic force models predict the cutting forces based on uncut chip load at the cutting edge. The cutting force predictions has become more and more closer to the experimental values by including various factors like tool geometry, operation type, tool vibrations etc in the force models (Altintas and Engin, 2001; Wu *et al.*, 2013). The forces for a general orthogonal cutting can be described by a mechanistic force model considering only cutting action of the cutting edge neglecting plowing and chisel edge effects. The machining force $\vec{F}_m$ is calculated considering the small finite elements of the cutting flute in the cutting edge referential frame decomposed: tangential (dF_t), radial (dF_r) and axial (dF_z) components for flute j is given by below equations:

$$d\vec{F}_m = \begin{bmatrix} dF_t \\ dF_r \\ dF_z \end{bmatrix} \tag{9}$$

Figure 2(b) illustrates the cutting forces exerted by the peripheral and bottom edges of the tool on the work piece during helical milling. The tangential, radial and axial force components are depicted at peripheral (F_{tp},F_{rp},F_{ap}) and bottom cutting edges (F_{tb}, F_{rb}, F_{ab}) respectively. However, the tangential (F_{tb}) and radial (F_{rb}) force components at the bottom edge is significantly small and can be neglected. The force components can be expressed as a function of uncut chip cross section and flute rotation angle θ_2 as:

$$F_{tp,j} = K_{tp}.h_p(\theta_2)_j b_p(\theta_2)_j \tag{10}$$
$$F_{rp,j} = K_{rp}.h_p(\theta_2)_j b_p(\theta_2)_j \tag{11}$$
$$F_{ap,j} = K_{ap}.h_p(\theta_2)_j b_p(\theta_2)_j \tag{12}$$
$$F_{ab,j} = K_{ab}.h_b R_t \tag{13}$$

where K_{tp},K_{rp},K_{ap} are the specific force coefficients for tangential, radial and axial force components obtained at peripheral cutting edge j and K_{ab} is the specific force coefficient from axial force component obtained at bottom cutting edge j. Hence the total force due to peripheral and bottom edges considering Z flutes in a tool can be expressed as below:

$$F_t = \sum_{j=1}^{Z} K_{tp}.h_p(\theta_2)_j b_p(\theta_2)_j \tag{14}$$
$$F_r = \sum_{j=1}^{Z} K_{rp}.h_p(\theta_2)_j b_p(\theta_2)_j \tag{15}$$
$$F_a = \sum_{j=1}^{Z} K_{ap}.h_p(\theta_2)_j b_p(\theta_2)_j + Z.K_{ab}.h_b R_t \tag{16}$$

However, during experiments, the cutting forces recorded are in work piece referential (F_{xm}, F_{ym}, F_{zm}) and can be transferred to one of the reference cutting edges. The reference flute position (θ_2) being known, the angular position of remaining flutes for a particular tool can be calculated:

$$(\theta_2)_j = (\theta_2) + (j-1)\lambda \tag{17}$$

where λ=$2\pi/Z$ is the tool pitch angle The axial components (F_{ap}+F_{ab}) can be approximated to cutting force (F_{zm}) obtained in Z direction during experiments. The rotation matrix for transformation of forces is given by Eq.18:

$$\begin{bmatrix} F_r(\theta_2)_j \\ -F_t(\theta_2)_j \\ F_a \end{bmatrix} = \begin{bmatrix} \cos(-\theta_2)_j & -\sin(-\theta_2)_j & 0 \\ \sin(-\theta_2)_j & \cos(-\theta_2)_j & 0 \\ 0 & 0 & 1 \end{bmatrix} . \begin{bmatrix} F_X \\ F_Y \\ F_Z \end{bmatrix} \tag{18}$$

2.4 Cutting power model

In case of end milling, the cutting power is summation of power consumed by all the flutes ($j = 1..Z$) in active contact with the work piece at any instant of time. $Power_p$ and $Power_b$ denotes cutting power because of peripheral and bottom cutting edges respectively which are in active contact with the work piece :

$$Power_{cut} = \sum_{j=1}^{Z} [Power_p(j) + Power_b(j)] \tag{19}$$

Depending upon the cutter pitch angle, the number of peripheral flutes simultaneously in contact with the work piece can be determined considering peripheral angle of immersion between ϕ= 0 to 180^o for helical milling. It is important to note that the bottom edges of all the flutes are always in contact with the work piece during helical milling. Tangential force component F_{tp} at the peripheral cutting edge is the major component of cutting force in magnitude and can be considered for the calculation of cutting power $Power_p$ at peripheral edge. Similarly, axial force component F_{ab} is the major cutting force at the bottom edge and can be used to express cutting power $Power_b$ at bottom edge of the tool. Hence cutting power can be expressed approximately as a function of cutting force and cutting velocity V_c. The cutting velocity at a point on the bottom edge varies along the edge based on its distance from the tool center. Hence the cutting power is expressed as a function of average cutting velocity $\overline{V}_c$ for the bottom cutting edges as shown below:

$$Power_{cut} = \sum_{j=1}^{Z} \frac{1}{60} \Big\{ g(\theta_2)_j \cdot (F_{tp})_j \cdot V_c + (F_{ab})_j \cdot \overline{V}_c \Big\} \tag{20}$$

where $g(\theta_2)$=0 or 1 is a contact function based on position of the peripheral flute in or out of immersion angle zone. Tangential F_{tp} and axial F_{ab} force components can be further expressed as a function of specific force coefficients (K_{tp},K_{ab}) and uncut chip load (h_p, b_p, h_b, b_b) as follows:

$$Power_{cut} = \sum_{j=1}^{Z} \frac{1}{60} \Big\{ g(\theta_2)_j \cdot [h_p(\theta_2) \cdot b_p(\theta_2)]_j \cdot K_{tp} \cdot V_c + [h_b \cdot b_b]_j \cdot K_{ab} \cdot \overline{V}_c \Big\} \tag{21}$$

2.5 Identification of specific force parameters using power

Machine spindle power can be monitored during machining and can have significant information for decision making process. The total spindle power monitored has components of cutting, non cutting or idle power because of spindle inertia and power because of tool feed motion as shown in the Fig. 3. The total spindle power can be expressed as:

$$Power_{total} = Power_{idle} + Power_{cut} + Power_{feed} \tag{22}$$

The idle power component for a particular machine spindle can be determined during experiments by recording non cutting spindle power. The power because of tool feed motion is assumed to be relatively less in helical milling. During experiments, $power_{total}$ can be recorded for different known values of θ_2 at pre defined cutting conditions.The modelled cutting power Eq. 21 can be re-written to determine values of K_{tp} and K_{ab} as a function of cutting power and chip dimensions.

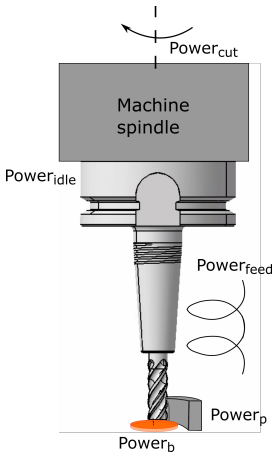

Figure 3: Spindle power components

3. MATERIALS AND METHODS

The aim of the experiment is to monitor spindle power for material identification during hole making of stacked aerospace materials. Cutting forces are also recorded using a dynamometer to compare with the power signal especially at material interface to verify changes in gradient of signals. However, the main goal is to utilize CNC machine internal sensors for material identification considering the advantages of easier implementation on industrial shop floor. Helical milling experiments were carried out on most commonly used aerospace stacks made of Aluminium (2017A) and Titanium (Ti6Al4V) alloy at different cutting conditions. The experimental setup is described in the following subsections.

3.1 Experimental setup

Experiments were carried out on a CNC milling center DMU85-DMG mono block machine under wet condition. A carbide end mill from *Fraisa* with 4 flutes and 8 mm diameter was used for all the helical milling experiments. The stack is made of Aluminium (2024A) and Titanium (Ti6Al4V) alloy with 4 mm thickness of each layer bearing dimensions 35 mm X 100 mm. The material layers are fastened together by bolt/nut assembly using a fixture as shown in the Fig. 4(a). The stack sequence is varied during experiments and represented as Al$\rightarrow$ Ti for Aluminium Titanium sequence and Ti$\rightarrow$ Al for Titanium Aluminium sequence. The work piece is fixed on a 9257B Kistler dynamometer, inside the internal measuring region, connected to a 5070 *Kistler* amplifier. Analogical data of force is converted to digital using a 9201 *National Instruments* acquisition module using 1000 Hz acquisition rate. For power acquisition, *Sinucom NC trace* software tool which can monitor spindle power at a rate of 4 ms is utilised. Along with spindle power, tool position data from CNC machine $(X1, Y1, Z1)$ and spindle angular position SP is also recorded. The relation between SP and θ_2 is discussed in the next subsection.

An external photoelectric sensor (*WL150-P132 from Sick*) is setup to identify cutting flute position by placing a reflective tape just above the cutting flute as shown in the Fig.4(b). The sensor is connected to NI data acquisition card 9215 via BNC cable. Sensor data is read and written on *Labview* software connected to NI DAQ via USB cable. The working principle of the sensor and cutting flute identification is also detailed in the next subsection.

3.2 Cutting flute position identification

The described photoelectric sensor is set up to identify the reference cutting flute position (θ_2) in real time by comparing it with the monitored machine spindle position SP. Spindle position values $(0 - 360^o)$ is tracked by *Sinucom Trace* package and recorded on a laptop connected to the CNC machine through Ethernet cable. It is significant to note that the spindle position values recorded is the spindle angular orientation with respect to machine builders reference for a particular machine. The recorded values may not directly represent cutting flute position as this depends upon the actual orientation of the flute inside a tool holder as shown in the Fig.5.

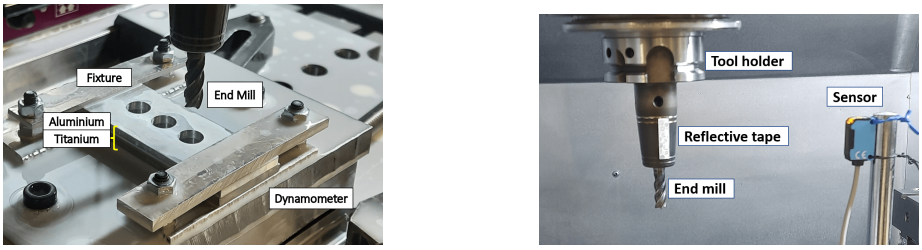

(a) Al/Ti stack (b) Sensor setup

Figure 4: Experimental setup

Figure 5(a) depicts a tool with four flutes and also having the reference cutting flute aligned with the machine spindle reference position. In this case, the traced angular values of machine spindle can be approximated as equal to reference cutting flute position angular values (θ_2). The corresponding position angle of remaining flutes can be determined by adding pitch angle to obtained θ_2 values based on the number of flutes in the tool.

However, Fig.5(b) shows an end mill where the reference cutting flute position is unaligned with machine spindle position reference and there is an angular difference of δ between the reference cutting flute and spindle position reference. The δ angular correction has to be applied in order to determine correct reference flute position (θ_2).

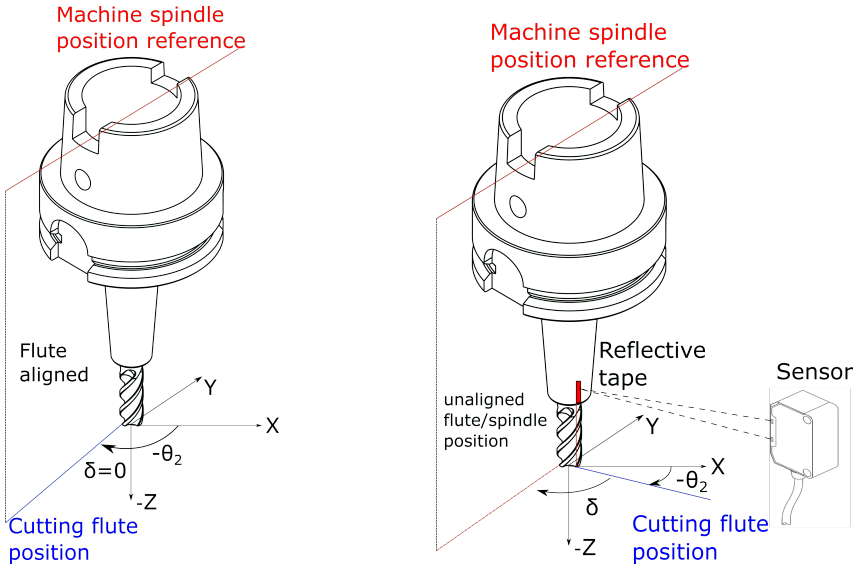

(a) Spindle position (SP) (b) Reference cutting edge position θ_2

Figure 5: Identification of reference flute position

The identification of δ is possible by the photoelectric sensor which gives a voltage high as it encounters the reflective tape placed directly above the reference cutting flute as shown in the Fig. 5(b). The machine spindle position values ($0 - 360^o$) are also simultaneously recorded during this time interval. The clock on the CNC machine and the sensor connected to *Labview* is set identical before recording the values of spindle position and flute position. The set of data points having common time stamps from both the systems is then super imposed as shown in the Fig. 6 to identify angular difference between the reference cutting flute and spindle encoder reference position. The sensor signal peak (voltage high) in the graph denotes reference cutting flute detection and the corresponding value of the spindle position is found to be around 297^o. This δ value is offset from the recorded machine spindle position values in order to get real time reference cutting flute position (θ_2) by real time data monitoring. This method involves integrating data from two different platforms and the determined δ value is just an approximation for establishing θ_2.

The cutting coefficients calculated by approximating θ_2 values in both the cases, (i.e reference flute aligned with machine spindle reference and unaligned reference flute where sensor is used to approximate flute position) has identical values and similar data maps.

3.3 Design of Experiments

Table **??** summarizes the cutting conditions adopted for helical milling experiments and the stack sequence of Aluminium and Titanium alloy for each test. The cutting velocity (V_c) is 40 m/min for all the experiments and a range of feed per tooth in axial (f_a) and trajectory (f_z) is defined resulting in different N_{orb} and $pitch$. A 11 mm diameter hole (through hole) is produced in the stacks by helical milling. The cutting velocity is opted considering machining of two

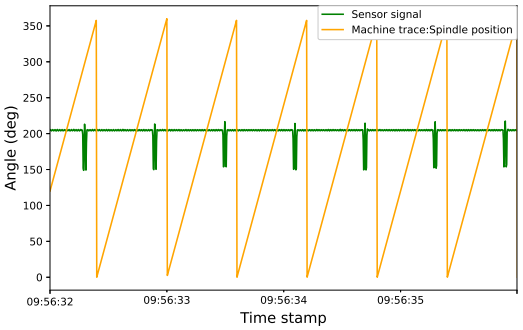

Figure 6: Identification of δ

Table 1: Cutting conditions

Stack	f_a *(mm/th)*	f_z *(mm/th)*	V_c *(m/min)*	N_{orb} *(rev/min)*	P *(mm/rev)*
Ti→ Al	0.002	0.044	40	30	0.5
Ti→Al	0.003	0.059		40	
Al→Ti	0.002	0.044		30	
Al→Ti	0.003	0.059		40	
Ti→Al	0.001	0.044		30	0.3
Ti→Al	0.002	0.059		40	

different materials layers and $11mm$ diameter hole being one of the most commonly produced hole diameters in aerospace industry.

4. EXPERIMENTAL RESULTS

The following subsections present the cutting power, cutting forces monitored during helical milling of stacks and estimated specific force coefficients data map using cutting power. The data maps of specific coefficients show distinct data points indicating different materials and can be advantageous for material identification especially at interface layers of different material (Deshpande *et al.*, 2022b). Cutting power is monitored by utilizing machine internal sensors while cutting forces is monitored by external sensor (Dynamometer) simultaneously, However, specific coefficients are estimated from cutting power signal and this is to verify the possibility of utilising spindle power for material identification. Cutting forces are presented to compare with the power signal especially at material interface to verify material transition at a specific hole length in both the signals.

4.1 Cutting power

Figure 7 shows cutting power as a function of hole depth at various feed per tooth and stack sequences. The material layers can be approximately identified by the distinct steps observed in the power signal at the stack interface approximately at $4mm$ where tool transition occurs from one layer to another. It can be seen from the Fig. 7 (c) and (d) that the tool transition from Titanium to Aluminium shows distinct peaks especially at the layer interface. Figure 7 (d) shows further disturbances in the signal during machining of Aluminium and its difficult to approximate two different material layers. This can be mostly attributed to sticky chips of Titanium sticking to the cutting edge which is re-machined while machining Aluminium. This phenomenon is also reaffirmed in the cutting force signals observed during tool transition from Titanium to Aluminium layers which is shown in the next subsection. It is important to note that these signal disturbances were not consistent for all Ti→ Al stack sequence experiments but was observed frequently.

4.2 Cutting forces

Figure 8 shows the local cutting forces (F_t,F_r and F_a) obtained by transformation of experimental forces F_x, F_y and F_z by rotation matrix as shown in Eq.18. Here too, the signal peaks can be observed in Fig 8 (a), (b), (c) and (d) at the layer interface (at length $4mm$) while the tool is moving from one material layer to the other layer. However, it can be observed from Fig. 8 (d) that the axial force F_a at the Aluminium region is higher compared to Titanium region accompanied by signal disturbances which was also seen previously in the cutting power results for tool transition from Titanium layer to Aluminium layer.

4.3 Cutting force coefficients

Cutting force coefficients K_{tp} (at tool periphery) and K_{ab} (at tool bottom edge) are estimated from cutting power signal as described in subsection 2.5 The coefficients are calculated by taking maximum power values for every half orbital rotation of the tool and corresponding chip dimensions at that instant. K_{tp} and K_{ab} are represented as a function

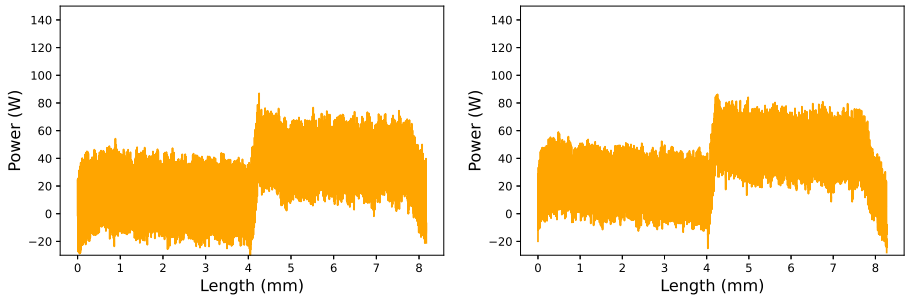

(a) Al→ Ti: f_a=0.002 mm/th, f_z=0.044 mm/th (b) Al→ Ti :f_a=0.003 mm/th, f_z=0.059 mm/th

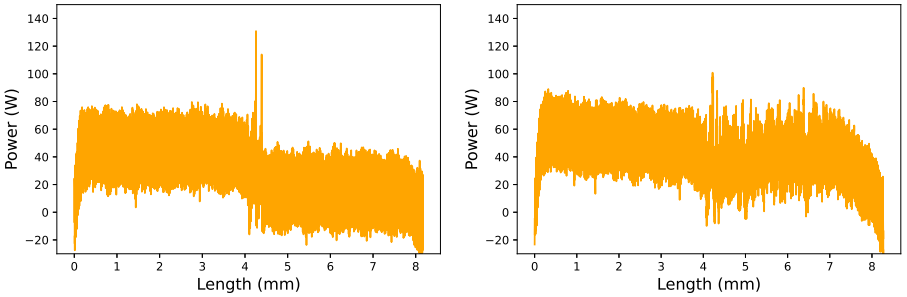

(c) Ti→ Al :f_a=0.002 mm/th, f_z=0.044 mm/th (d) Ti→ Al :f_a=0.003 mm/th, f_z=0.059 mm/th

Figure 7: Spindle power as a function of hole depth at different cutting conditions.

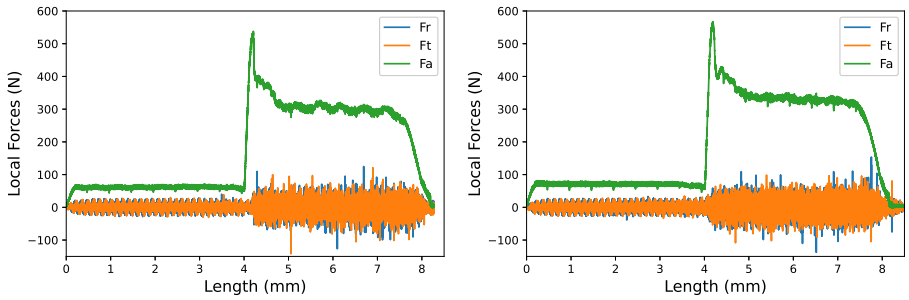

(a) Al→ Ti: f_a=0.002 mm/th, f_z=0.044 mm/th (b) Al→ Ti :f_a=0.003 mm/th, f_z=0.059 mm/th

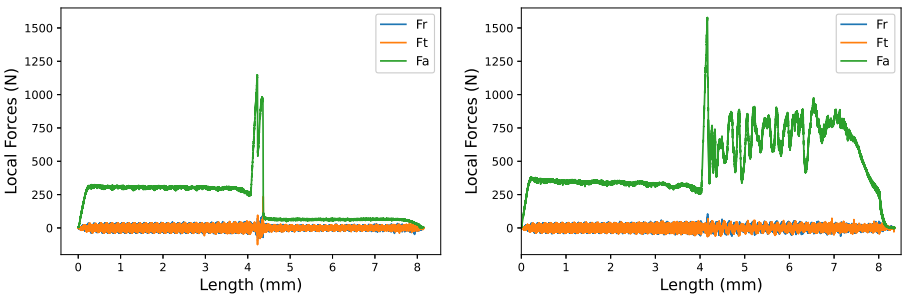

(c) Ti→ Al :f_a=0.002 mm/th, f_z=0.044 mm/th (d) Ti→ Al :f_a=0.003 mm/th, f_z=0.059 mm/th

Figure 8: Local cutting forces as a function of hole depth at different cutting conditions.

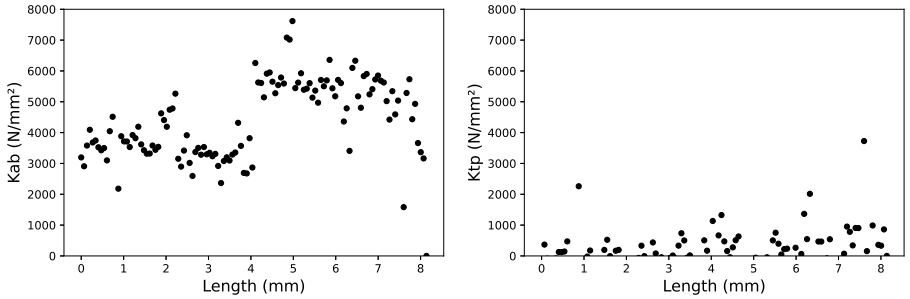

(a) K_{ab} at f_a=0.002 mm/th, f_z=0.044 mm/th (b) K_{tp} at f_a=0.002 mm/th, f_z=0.044 mm/th

Figure 9: Data map of cutting force coefficients for Al→ Ti stack

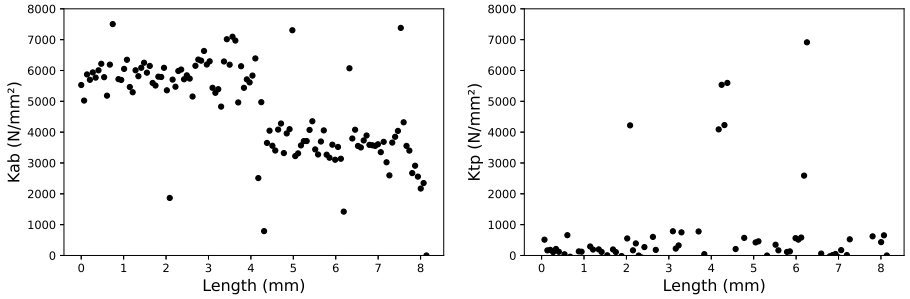

(a) K_{ab} at f_a=0.002 mm/th, f_z=0.044 mm/th (b) K_{tp} at f_a=0.002 mm/th, f_z=0.044 mm/th

Figure 10: Data map of cutting force coefficients for Ti→ Al stack

of hole depth for different stack sequence as shown in the Fig. 9 and 10. The values of K_{ab} for both the material layers can be seen in the Fig. 9 (a) and 10 (a) and these data points indicate stacked materials of different machinability. The data points observed in Fig. 10 (a) has some unpredictable values when the tool moves from Titanium to Aluminium layer. This may be attributed to sticky Titanium chips at the cutting edge being re-machined at the Aluminium layer. However, we can still distinguish two different material layers from the data map of K_{ab}. Figure 9 (b) and 10 (b) shows the tangential cutting force coefficient K_{tp} for both the material layers at f_a=0.002 mm/th and f_z=0.044 mm/th. It is difficult to distinguish two different material layers by observing K_{tp} values as the data points are distributed through out the length of the stack without any distinct region of data points.

5. CONCLUSIONS

Our work validates the possibility of material identification by data maps during orbital drilling of stacked Aluminium and Titanium alloys. These data maps are developed by online data monitoring utilizing machine internal sensor to monitor spindle power and an external photoelectric sensor to detect flute position. The data map of axial cutting force coefficient (K_{ab}) has distinct data points distinguishing two separate regions in the map indicating two separate material layers. However, it is difficult to identify two different material layers by observing data map of tangential cutting force coefficient (K_{tp}) as the data points are unevenly distributed without any specific regions for different material layers.

The stack sequence also plays a crucial role in terms of generated cutting forces and required cutter power for machining. Especially, the transition of tool from Titanium to Aluminium layer is accompanied by disturbances in monitored signal of cutting force and power. This may lead to improper value of data points which in turn result in erroneous material identification. However, if there is a small delay in identification of Aluminium while the tool is transiting from Titanium, it does not result in any catastrophic loss of the tool. The consequences of stack sequence on data maps needs further studies. Our work also demonstrates utilization of machine internal sensors for online data monitoring as a substitute to external expensive sensors and can be explored further for industrial applications on shop floor. The map of cutting force coefficients can be used to train machine learning models in the future for smart machining applications including adapting proper cutting parameter suitable for a particular layer.

6. REFERENCES

Al-Naggar, Y.M., Jamil, N., Hassan, M.F. and Yusoff, A.R., 2021. "Condition monitoring based on IoT for predictive maintenance of CNC machines". *Procedia CIRP*, Vol. 102, pp. 314–318.

Altintas, Y. and Engin, S., 2001. "Generalized Modeling of Mechanics and Dynamics of Milling Cutters". *CIRP Annals*, Vol. 50, pp. 25–30.

Araujo, A.C., Landon, Y. and Lagarrigue, P., 2021. "Smart drilling for Aerospace Industry: state of art in research and education". *Procedia CIRP*, Vol. 99, pp. 387–391.

Axinte, D. and Gindy, N., 2004. "Assessment of the effectiveness of a spindle power signal for tool condition monitoring in machining processes". *International Journal of Production Research*, Vol. 42, No. 13, pp. 2679–2691.

Boyer, R.R., Cotton, J.D., Mohaghegh, M. and Schafrik, R.E., 2015. "Materials considerations for aerospace applications". *MRS Bulletin*, Vol. 40, No. 12, pp. 1055–1066.

Dan Sun, Patrick Lemoine, D.K.e.a., 2018. "Hole-making processes and their impacts on the microstructure and fatigue response of aircraft alloys". *The International Journal of Advanced Manufacturing Technology*, Vol. 94, p. 1719–1726.

Demko, M., Vrabeľ, M., Maňková, I. and Ižol, P., 2022. "Cutting tool monitoring while drilling using internal CNC data". *Procedia CIRP*, Vol. 112.

Denkena, B., Boehnke, D. and Dege, J.H., 2008. "Helical milling of CFRP–titanium layer compounds". *CIRP Journal of Manufacturing Science and Technology*, Vol. 1, pp. 64–69.

Deshpande, S., Araujo, A.C., Lagarrigue, P. and Landon, Y., 2022a. "Experimental analysis of circular milling for material identification in aerospace industry". *Key Engineering Materials*, Vol. 926, pp. 1650–1659.

Deshpande, S., Coimbra Gonçalves, M.C., Araujo, A.C., Lagarrigue, P. and Landon, Y., 2022b. "Specific force map for smart machining applications with rotating tools". *Proceedings of the Institution of Mechanical Engineers, Part B: Journal of Engineering Manufacture*. Publisher: IMECHE.

Fang, Q., Pan, Z.M., Han, B., Fei, S.H., Xu, G.H. and Ke, Y.L., 2015. "A Force Sensorless Method for CFRP/Ti Stack Interface Detection during Robotic Orbital Drilling Operations". *Mathematical Problems in Engineering*, Vol. 2015, pp. 1–11.

Ge, J., Reji, R., Feist, T., Elmore, A., McClelland, J., Higgins, C., McLaughlin, B., Jin, Y. and Sun, D., 2022. "Investigating hole making performance of Al 2024-T3/Ti-6Al-4V alloy stacks: A comparative study of conventional drilling, peck drilling and helical milling". *The International Journal of Advanced Manufacturing Technology*, pp. 5027–5040.

Lauro, C.H., Brandão, L.C., Baldo, D., Reis, R.A. and Davim, J.P., 2014. "Monitoring and processing signal applied in machining processes – a review". *Measurement*, Vol. 58, pp. 73–86.

Liu, C., Vengayil, H., Lu, Y. and Xu, X., 2019. "A Cyber-Physical Machine Tools Platform using OPC UA and MTConnect". *Journal of Manufacturing Systems*, Vol. 51, pp. 61–74. ISSN 0278-6125.

Martellotti, M.E., 1941. "An analysis of the milling process". *Trans. ASME*, pp. 677–687.

Neugebauer, R., Ben-Hanan, U., Ihlenfeldt, S., Wabner, M. and Stoll, A., 2012. "Acoustic emission as a tool for identifying drill position in fiber-reinforced plastic and aluminum stacks". *International Journal of Machine Tools and Manufacture*, Vol. 57, pp. 20–26.

Pardo, A., Heinemann, R., Nobre, N.M. and Bagshaw, L., 2021. "Assessment of decision-making algorithms for adaptive drilling of aerospace stacks". *Procedia CIRP*, Vol. 99, pp. 392–397.

Rey, P.A., LeDref, J., Senatore, J. and Landon, Y., 2016. "Modelling of cutting forces in orbital drilling of titanium alloy Ti–6Al–4V". *International Journal of Machine Tools and Manufacture*, Vol. 106, pp. 75–88.

Shang, S., Qin, X.D., Li, J.H., Li, S.P., Li, H., Huang, T., Jin, Y. and Sun, D., 2018. "Modelling of cutting forces and researching calibration method in helical milling". *The International Journal of Advanced Manufacturing Technology*, Vol. 94, pp. 2949–2960.

Vijayan, K., Zitoune, R. and Collombet, F., 2010. "Comprehensive Review on Drilling of Multimaterials Stacks". *Journal of Machining and Forming Technologies*, Vol. 2, No. 3/4, pp. 171–200.

Wang, G.D., Suntoo, D., Li, N., Peng, T. and Li, Y., 2018. "Experimental research in CFRP/Ti stack through different helical milling strategies". *The International Journal of Advanced Manufacturing Technology*, Vol. 98, pp. 3251–3267.

Wang, H., Qin, X., Ren, C. and Wang, Q., 2012. "Prediction of cutting forces in helical milling process". *The International Journal of Advanced Manufacturing Technology*, Vol. 58, No. 9, pp. 849–859.

Wu, B., Yan, X., Luo, M. and Gao, G., 2013. "Cutting force prediction for circular end milling process". *Chinese Journal of Aeronautics*, Vol. 26, pp. 1057–1063.

Zhaoju, Z., Liu, K., Sun, J. and Li, J., 2017. "Investigation on performance characteristics and metallographic transformation on drilling aluminium/titanium sandwich". *Journal of Sandwich Structures and Materials*, Vol. 21.

7. INFORMATION'S RESPONSIBILITY

The authors are responsible for the information included in this work.